Available online at www.sciencedirect.com
ScienceDirect
Solar Energy Materials & Solar Cells 91 (2007) 17–28
Solar Energy Materials and Solar Cells
www.elsevier.com/locate/solmat

Parametric study of various configurations of hybrid PV/thermal air collector: Experimental validation of theoretical model

Arvind Tiwari*, M.S. Sodha

Center for Energy Studies, Indian Institute of Technology, New Delhi 110016, India

Received 3 February 2006; received in revised form 30 March 2006; accepted 12 June 2006
Available online 12 September 2006

Abstract

In this paper, an attempt has been made to evaluate the overall performance of hybrid PV/thermal (PV/T) air collector. The different configurations of hybrid air collectors which are considered as unglazed and glazed PV/T air heaters, with and without tedlar. Analytical expressions for the temperatures of solar cells, back surface of the module, outlet air and the rate of extraction of useful thermal energy from hybrid PV/T air collectors have been derived. Further an analytical expression similar to Hottel–Whiller–Bliss (HWB) equation for flat plate collector has also been derived in terms of design and climatic parameters. Numerical computations have been carried out for composite climate of New Delhi and the results for different configurations have been compared. The thermal model for unglazed PV/T air heating system has also been validated experimentally for summer climatic conditions. It is observed that glazed hybrid PV/T without tedlar gives the best performance.
© 2006 Elsevier B.V. All rights reserved.

Keywords: Hybrid PV/thermal; Air heating systems and solar energy

1. Introduction

A thermal model, predicting the temperature of photovoltaic (PV) in a panel, as a function of climatic parameters under non-steady-state conditions, has been developed and validated experimentally [1]. It is seen that the module temperature goes up to 325 K for clear sky conditions in the month of September in Newcastle, UK. If significant part of incident solar energy is withdrawn to lower the module temperature, the efficiency of the module can be increased [2]. The withdrawal of thermal energy can be conveniently carried out by the flow of a fluid below the PV module. The fluid can be either water or air, as per system requirements. Many experimental and theoretical studies have been reported for

(a) hybrid PV/thermal (PV/T)water heating system [2–8],
(b) hybrid PV/T air heating system [9–12].

Recently, Infield et al. [10] have studied the thermal performance of ventilated PV facades with the PV panel, exposed to solar radiation and double-glazed surface facing room air. The air is allowed to flow through the duct at a flow rate of 0.3 m/s. They observed that the thermal efficiency of a PV facade is about 25.8% under European climatic conditions for the month of August 2000. Further, Hegazy [9] has studied four configurations of PV/T solar air collectors and observed that the configuration with air flow between top glass cover and solar cell gives an overall (electrical and thermal) efficiency of about 55% at 0.04 kg/m^2 s mass flow rate of air. Radziemska [13] has reviewed the work on air- and water-cooled hybrid PV/T solar air collector which includes the work done by Tripanagnostopulos et al. [6] and Prakash [11].

Exergy analysis of PV/T system has been carried out by Bosonac et al. [14] on the basis of the second law of thermodynamics [15]. The exergy efficiency is lower than energy efficiency and this depends on the operating temperature of PV/T system.

*Corresponding author. Tel.: +91 11 26591255.
E-mail address: arvindtiwari02@yahoo.com (A. Tiwari).

0927-0248/$ - see front matter © 2006 Elsevier B.V. All rights reserved.
doi:10.1016/j.solmat.2006.06.061

Nomenclature

A	area, m^2
b	breadth, m
C	specific heat, J/kg °C
dx	elemental length, m
F_R	flow rate factor
h	heat transfer coefficient, W/m^2 °C
h_{p1}	penalty factor
h_{p2}	penalty factor
$I(t)$	incident solar intensity, W/m^2
K	thermal conductivity, W/m °C
L	length, m
M	mass, kg
$\dot{m}$	rate of flow of air mass,
n	number of observations
$\dot{Q}_u$	rate of useful energy transfer, MJ
t	time, s
T	temperature, °C
U_b	an overall heat transfer coefficient from bottom to ambient
U_L	an overall heat transfer coefficient from solar cell to ambient through top and back surface of insulation
U_t	an overall heat transfer coefficient from solar cell to ambient through glass cover
U_T	conductive heat transfer coefficient from solar cell to air through tedlar
U_{tT}	an overall heat transfer coefficient from glass to tedlar through solar cell
X	theoretical value
X_i	theoretical value of ith term
Y	experimental value
Y_i	experimental value of ith term

Subscripts

O	glass to ambient
a	ambient
bs	back surface of tedlar
c	solar cell
eff	effective
g	glazing
G	glass
i	insulation
r	reference
T	tedlar
th	thermal

Greek letters

α	absorptivity
β	packing factor
η	efficiency
τ	transmitivity

In this paper, an attempt has been made to evaluate an overall thermal efficiency of the following configuration of PV/T solar air heating systems:

(a) unglazed hybrid PV/T with tedlar, Model I, Fig. 1a(i),
(b) unglazed hybrid PV/T without tedlar, Model II, Fig. 1a(ii),
(c) glazed hybrid PV/T with tedlar, Model III, Fig. 1b(i),
(d) glazed hybrid PV/T without tedlar, Model IV, Fig. 1b(ii).

The methodology adopted for analyzing the unglazed hybrid PV/T solar air collector by Tiwari et al. [16] has been considered in this paper.

The thermal circuit diagram of each model has been shown in Fig. 2.

2. Experimental set-up [16]

Two modules are connected in series. Each module has an effective area of 0.61 m^2. Both modules have been mounted on a wooden structure with air duct at back of module. There was a provision to pass air through the duct as shown in Fig. 3a. The system has been placed over a steel frame with variable inclination. For the present experiment, the inclination of module has been fixed at 30° to the horizontal. The air duct was sealed with the help of putty and double-side tape to avoid hot air leakage. The temperature sensors have been used to measure the various temperatures of namely the solar cells, back surface of module, inlet air and outlet air. One temperature sensor has also been provided at the top surface of the module to measure the temperature of the exposed surface of PV module. Air has been passed through the duct by using two fans of capacity 12 W at inlet, upper end of the duct. The fans are operated by DC battery (12 V and 120 Ah) as shown in Fig. 3b.

2.1. Experimental parameters [16]

Following are the specifications of the solar cell and the module:

(a) *Solar cell*: The solar cell has the following specifications at $I(t) = 1000\,W/m^2$ at a cell temperature of 25 °C; Fill factor = 0.72, $I_{sc} = 4.8\,A$, $V_{oc} = 600\,mV$, $I_d = 1000\,W/m^2$, area = 0.0139 m^2 and electrical efficiency (η) = 15%.
(b) *PV module*: The module has the following specifications:
$I_{max} = 4.4$ A, $V_{max} = 17\,V$, $I_d = 1000\,W/m^2$, area of one module = 0.61 m^2, electrical efficiency (η) = 12% and packing factor = 83%.

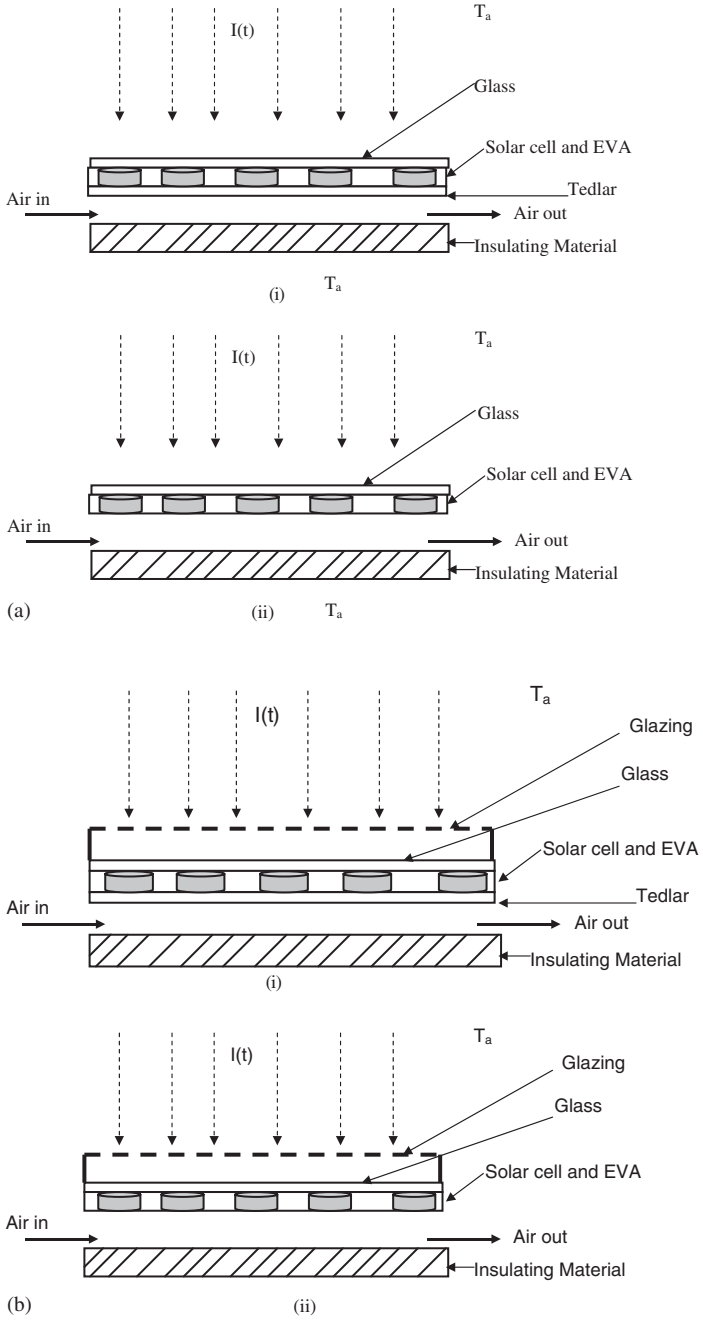

Fig. 1. (a) Cross-sectional view of unglazed PV/thermal air (i) with tedlar (Model I) [16], (ii) without tedlar (Model II). (b) Cross-sectional view of glazed PV/thermal air (i) with tedlar (Model III), (ii) without tedlar (Model IV).

(c) *Hybrid system*: The system has the following design parameters:
$b = 0.45\,\text{m}$, $L = 1.2\,\text{m}$, $\tau_G = 0.95$, $\tau = 0.9$.
The other parameters are:

$\alpha_c = 0.9$, $\beta_c = 0.83$, $\alpha_T = 0.5$, $(\alpha\tau)_{\text{eff}} = 0.656$,
$h_c = 7.98\,\text{W/m}^2\,^\circ\text{C}$, $h_r = 3.47\,\text{W/m}^2\,^\circ\text{C}$, $L_i = 0.05\,\text{m}$,
$L_c = 0.0003\,\text{m}$, $L_T = 0.0005\,\text{m}$, $L_G = 0.003\,\text{m}$,
$L_g = 0.003\,\text{m}$, $K_i = 0.035\,\text{W/m}\,^\circ\text{C}$, $K_c = 0.039\,\text{W/m}\,^\circ\text{C}$,
$K_T = 0.033\,\text{W/m}\,^\circ\text{C}$, $K_G = 1\,\text{W/m}\,^\circ\text{C}$,
$K_g = 0.04\,\text{W/m}\,^\circ\text{C}$.

2.2. Experimental observations

The experiment has been conducted under forced mode of operation during the summer month of year 2004 with a single fan. Hourly variation of solar intensity, ambient temperature, wind and duct air velocity and various

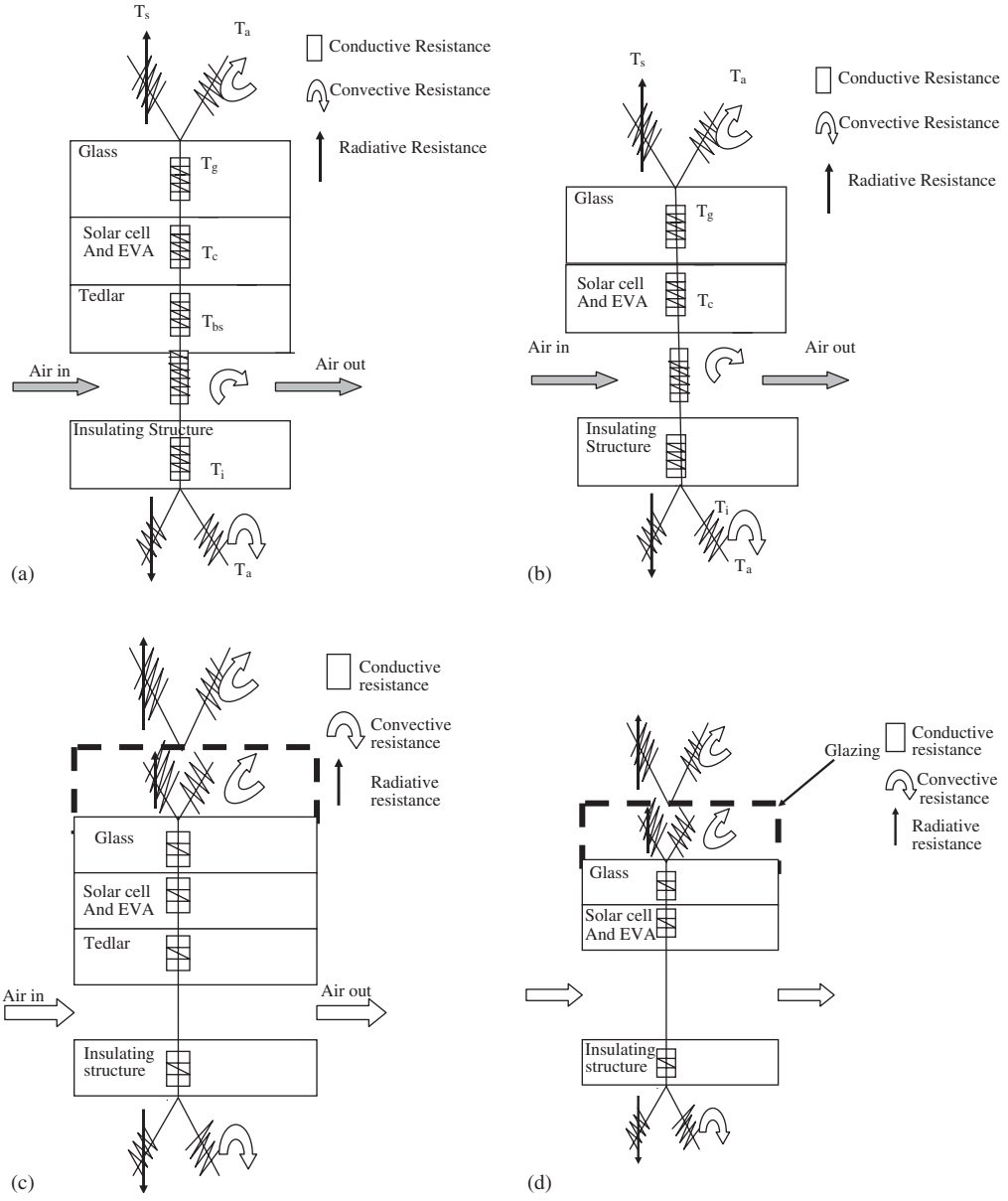

Fig. 2. (a) Thermal resistance circuit diagram for unglazed PV/thermal air with tedlar (Model I) [16]. (b) Thermal resistance circuit diagram for unglazed PV/thermal air without tedlar (Model II). (c) Thermal resistance circuit diagram for glazed PV/thermal air with tedlar (Model III). (d) Thermal resistance circuit diagram for glazed PV/thermal air without tedlar (Model IV).

temperatures has been recorded during the sunshine hours. The hourly data for a typical day of the month of July 2004 have been given in Table 1a and b.

3. Theoretical analysis

In order to write an energy balance for each component of four configurations mentioned above, the following assumptions have been made:

(i) There is no temperature gradient across the thickness of glass cover, solar cell, and tedlar and air column.
(ii) There is stream line flow of air through the duct.
(iii) The system is in a quasi-steady state condition.
(iv) The heat transfer coefficient is constant during the temperature range under study.
(v) Ohmic losses in solar cell are negligible.

3.1. Single hybrid PV/T module for a given length, L

The energy balance equations are based on the thermal resistance circuit diagram of each case as shown in Fig. 3 [16].

Model I: Unglazed PV/T air with tedlar [16] (Figs. 1a (i) and 3a) [16].

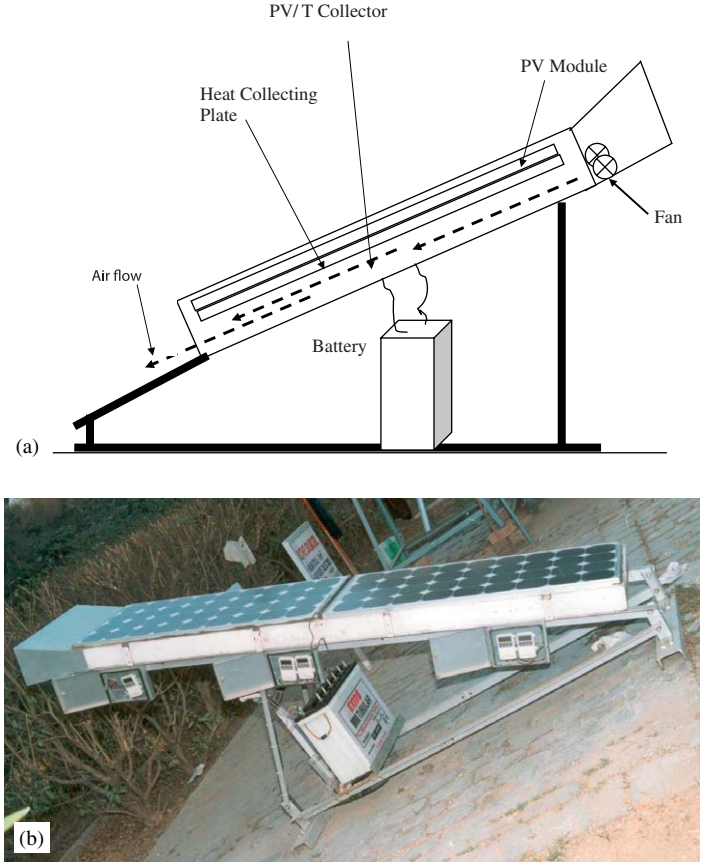

Fig. 3. (a) Schematic diagram of hybrid PV/thermal system. (b) Side view of hybrid PV/thermal system.

Table 1a
Hourly variation of climatic parameter and various temperatures (July 13, 2004)

Time (h)	Intensity (W/m^2)	Ambient temperature (°C)	Panel-1 temperature (°C)		Panel-2 back surface temperature (°C)	Outlet air temperature (°C)	Inlet air temperature (°C)
			Back surface	Front surface			
9	366	31	42.9	42	36.4	36.6	34.2
10	528	33	44	44.3	38.6	37.9	35.1
11	704	34	50.1	48.5	42.4	41.4	37.7
12	660	36	49.5	51.3	42.8	41.5	38.2
1	639	36	51.3	54.7	44.2	42.6	38.7
2	323	36	46.1	49.9	42	40.6	37.8
3	167	35	44.5	47.1	41.4	35.8	37.4
4	298	36	42.9	45	40.4	39.4	37.7

Table 1b
Hourly variation of voltage, current and wind velocity (July 13, 2004)

Time (h)	Short circuit current (A)	Open circuit voltage (V)	Load current (A)	Load voltage (V)	Air velocity (m/s)	
					In duct	Above PV module
9	−3.5	19.2	−1.3	13	2.83	0.83
10	−4.9	19.2	−2.1	13.2	3.9	1.5
11	−6.6	19	−2.1	13.5	4.3	0.98
12	−6.2	19	−2.1	13.4	4.83	1.52
1	−6.3	18.8	−2.1	13.5	4.47	0
2	−4.4	18.9	−2.1	13.3	4.8	0.57
3	−1.8	18.3	−2.1	12.7	3.63	0
4	−3	18.9	−2.1	12.8	3.83	0

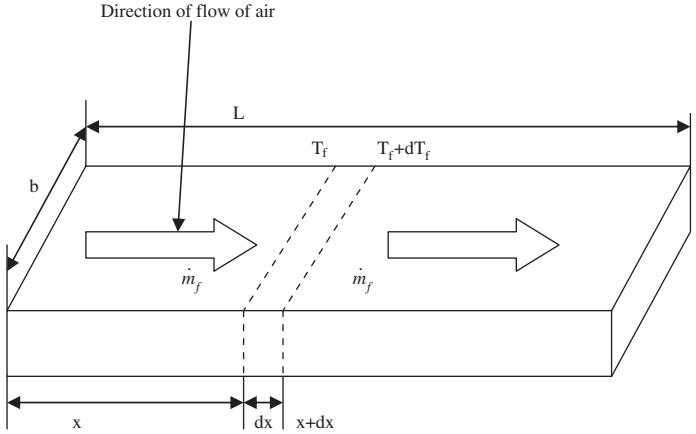

Fig. 4. Cross-sectional view of an elemental length 'dx' showing flow pattern of air below tedlar.

By considering an elemental area, $b\,\mathrm{d}x$, as shown in Fig. 4, one has

For PV module:

$$\tau_G[\alpha_c I(t)\beta_c + (1-\beta_c)\alpha_T I(t)]b\,\mathrm{d}x = [U_t(T_c - T_a) + U_T(T_c - T_{bs})]b\,\mathrm{d}x + \eta_c I(t)\beta_c b\,\mathrm{d}x, \quad (1)$$

where

$$U_t = \left[\frac{L_T}{K_T} + \frac{1}{h_0}\right]^{-1}.$$

For back surface of Tedlar:

$$U_T(T_c - T_{bs})b\,\mathrm{d}x = h_T(T_{bs} - T_{air})b\,\mathrm{d}x, \quad (2)$$

where

$$U_T = \frac{K_T}{L_T}.$$

For air flowing below the Tedlar:

$$h_T(T_{bs} - T_{air})b\,\mathrm{d}x = \dot{m}_a c_a \frac{\mathrm{d}T_{air}}{\mathrm{d}x}\,\mathrm{d}x + U_b(T_{air} - T_a)b\,\mathrm{d}x. \quad (3)$$

Model II: Unglazed PV/T air without tedlar (Figs. 1a (ii) and 3b).

For PV module:

$$\tau_G[\alpha_c I(t)\beta_c + (1-\beta_c)\alpha_{eva} I(t)]b\,\mathrm{d}x = [U_t(T_c - T_a) + h_T(T_c - T_{air})]b\,\mathrm{d}x + \eta_c I(t)\beta_c b\,\mathrm{d}x. \quad (4)$$

For air flowing below EVA:

$$h_T(T_c - T_{air})b\,\mathrm{d}x = \dot{m}_a c_a \frac{\mathrm{d}T_{air}}{\mathrm{d}x}\,\mathrm{d}x + U_b(T_{air} - T_a)b\,\mathrm{d}x. \quad (5)$$

Model III: glazed PV/T air with tedlar (Figs. 1b (i) and 3c).

For PV module:

Same as Eq. (1) with change in the expression for U_t as

$$U_t = \left[\frac{L_G}{K_G} + \frac{1}{h_c + h_r} + \frac{L_g}{K_g} + \frac{1}{h_0}\right]^{-1}. \quad (5a)$$

For back surface of Tedlar:

Same as Eq. (2).

For air flowing below Tedlar:

Same as Eq. (3).

Model IV: glazed PV/T air without tedlar (Figs. 1b (ii) and 3d).

For PV module:

Same as Eq. (4) with change in the expression for U_t as

$$U_t = \left[\frac{L_G}{K_G} + \frac{1}{h_c + h_r} + \frac{L_g}{K_g} + \frac{1}{h_0}\right]^{-1}. \quad (5b)$$

For air flowing below EVA:

Same as Eq. (5).

Eqs. (1)–(3) can be solved for the outlet air temperature (T_{airout}), back surface of module (T_{bs}) and solar cell (T_c) temperatures, [16]. Expression for these temperatures is as follows:

$$T_{airout} = T_{air}|_{x=L} = \left[\frac{h_{p1}h_{p2}(\alpha\tau)_{eff}I(t)}{U_L} + I(t)\right]\left(1 - e^{(-bU_L/\dot{m}_a c_a)L}\right) + T_{airin}\,e^{(-bU_L/\dot{m}_a c_a)L}, \quad (6a)$$

$$T_{bs} = \frac{h_{p1}(\alpha\tau)_{eff}I(t) + U_{tT}T_a + h_T T_{air}}{U_{tT} + h_T}, \quad (6b)$$

$$T_c = \frac{[\alpha_c\beta_c + \alpha_T(1-\beta_c)]I(t) - \eta_c I(t)\beta_c + U_t T_a + U_T T_{bs}}{U_t + U_T}. \quad (6c)$$

The average air temperature over the length of air duct below PV module is obtained as

$$\bar{T}_{air} = \frac{1}{L}\int_0^L T_{air}\,\mathrm{d}x = \left[\frac{h_{p1}h_{p2}(\alpha\tau)_{eff}I(t)}{U_L} + I(t)\right]\left(1 - \frac{1 - e^{(-bU_L/\dot{m}_a c_a)L}}{bU_L/\dot{m}_a c_a}\right) + T_{airin}\frac{1 - e^{(-bU_L/\dot{m}_a c_a)L}}{bU_L/\dot{m}_a c_a}. \quad (7a)$$

After knowing the average air temperature from the above equation, back surface of the module (T_{bs}) and solar cell (T_c), temperatures are obtained from Eqs. (6b) and (6c), respectively. Further, it is to be noted that electrical efficiency of solar cell depends on solar cell temperature as [17–18]

$$\eta = \eta_0[1 - 0.0045(T_c - T_0)]. \tag{7b}$$

Hence, a new value of solar cell efficiency is calculated for obtained value of cell temperature for known $\eta_0 = 0.12$ and $T_0 = 25\,^{\circ}\mathrm{C}$. Further, the whole calculation is repeated for the new value of solar cell efficiency. For second calculation of η, new value of solar cell efficiency becomes η_0 for first calculated value of T_c. This is done till the value of solar cell efficiency becomes constant.

The rate of useful thermal energy obtained from PV/T system is

$$\begin{aligned}\dot{q}_u &= \dot{m}_a c_a (T_{airout} - T_{airin}) \\ &= \frac{\dot{m}_a c_a}{U_L}\left\{h_{p1}h_{p2}(\alpha\tau)_{eff} I(t) - U_L(T_{airin} - T_a)\right\} \\ &\quad \times \left(1 - e^{(-bU_L/\dot{m}_a c_a)L}\right),\end{aligned} \tag{8}$$

where

$$U_L = U_{tair} + U_b,\ U_{tair} = \left[\frac{1}{U_{tT}} + \frac{1}{h_T}\right]^{-1},$$

$$U_{tT} = \left[\frac{1}{U_T} + \frac{1}{U_t}\right]^{-1},\ U_b = \left[\frac{L_i}{K_i} + \frac{1}{h_i}\right]^{-1},$$

$$h_{p1} = \frac{U_T}{U_t + U_T},\ h_{p2} = \frac{h_T}{U_{tT} + h_T},$$

$$(\alpha\tau)_{eff} = \tau_G\left\{\alpha_c\beta_c + \alpha_T(1 - \beta_c) - \eta_c\beta_c\right\}.$$

The overall efficiency, which includes electrical and thermal, of PV/T system is

$$\eta_O = \frac{\sum_{i=1}^{T}[\eta_c I(t)bL + \dot{q}_u]3600}{\sum_{i=1}^{T} I(t)bL3600}. \tag{9a}$$

or

$$\eta_O = \left[\eta_E + \frac{\sum_{i=1}^{T}\dot{q}_u}{\sum_{i=1}^{T} I(t)bL}\right]100 = [\eta_E + \eta_{TH}]100. \tag{9b}$$

If electrical efficiency, η_E, is converted to equivalent thermal efficiency, then, Eq. (9b) becomes

$$\eta_O = \left[\frac{\eta_E}{0.40} + \eta_{TH}\right]100. \tag{9c}$$

Here, the 0.40 factor is the conversion factor from thermal energy to electrical energy of the thermal power plant. In this case, an overall efficiency will be completely thermal efficiency.

The instantaneous thermal efficiency of a hybrid PV/T system is given by

$$\eta_i = \frac{\dot{q}}{I(t)bL} = \frac{\dot{m}_a c_a}{U_L bl} F_R\left\{h_{p1}h_{p2}(\alpha\tau)_{eff} - U_L\frac{(T_{airin} - T_a)}{I(t)}\right\}, \tag{10}$$

where $F_R = \left(1 - e^{(-bU_L/\dot{m}_a c_a)L}\right)$ is a flow rate factor.

Eq. (10), which is similar to Hottel–Whiller–Bliss (HWB) equation for flat plate collector can be used for testing of all configurations. Similar expression for Model II can be derived.

3.2. Two hybrid PV/T module connected in series for a given length, L

In this case two PV module, having equal length, are connected in series for total given length, L.

Energy balances of hybrid PV/T system and analytical expression for the outlet air temperature (T_{airout}), back surface of module (T_{bs}) and solar cell (T_c) temperatures, the rate of useful (Q_u) will remain the same, except T_{airin} of second module is replaced by T_{airout} of the first module. Other calculations remain the same.

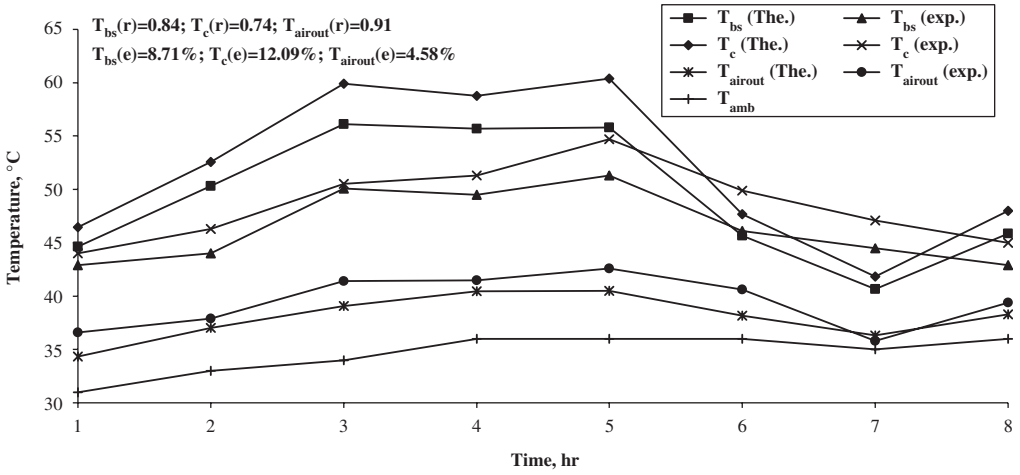

Fig. 5. Hourly variation of various temperatures with time.

4. Results and discussion

4.1. Experimental validation

The outlet air temperature (T_{airout}), back surface of module (T_{bs}) and solar cell (T_c) temperatures have been computed by using Eq. (6) and the Matlab program for the given design and climatic parameters (Tables 1a and b). The results for hourly variation have been shown in Fig. 5. The experimental results have also been shown in the same figure for comparison. It can be seen that there is fair agreement between theoretical and experimental values of outlet air with correlation coefficient (r) = 0.74 to 0.91 and standard percentage deviation error (e) = 4.58% to 12.09%. However, there is higher standard percentage deviation error (e) for back surface and solar cell temperatures. It may be due to drastic change in wind speed during experimentation.

4.2. Parametric studies

Eqs. (6) have been computed by the Matlab program for the outlet air temperature (T_{airout}), back surface of module (T_{bs}) and solar cell (T_c) temperatures for all four configurations and the results have been shown in Fig. 6. It is seen that the outlet air temperature (T_{airout}), back surface of module (T_{bs}) and solar cell (T_c) temperatures for module III, glazed hybrid PV/T with tedlar, Fig. 1c and Model IV, glazed hybrid PV/T without tedlar, Fig. 1d is significantly higher than the unglazed hybrid PV/T due to

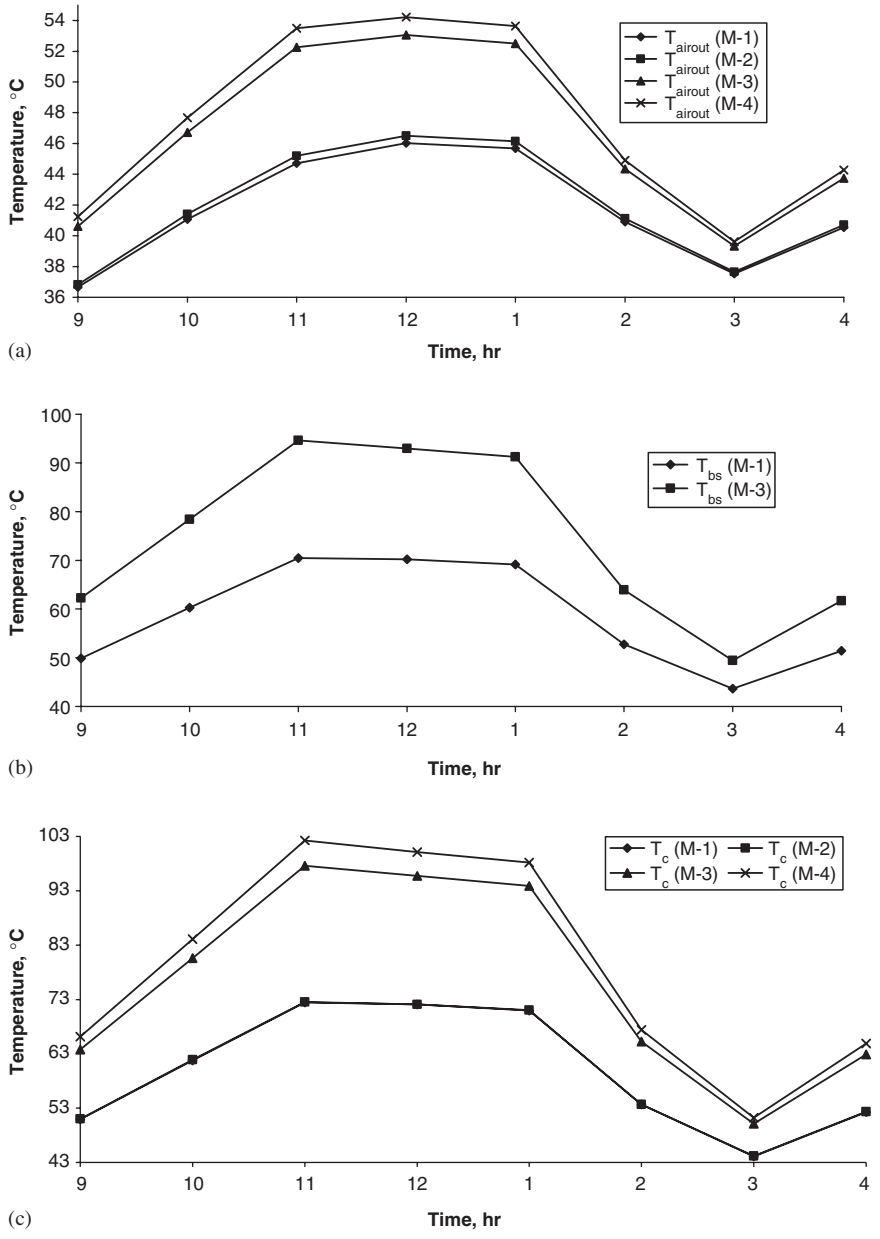

Fig. 6. (a) Hourly variation of outlet air temperature with time. (b) Hourly vairation of back surface temperature with time. (c) Variation of solarcell temperature with time.

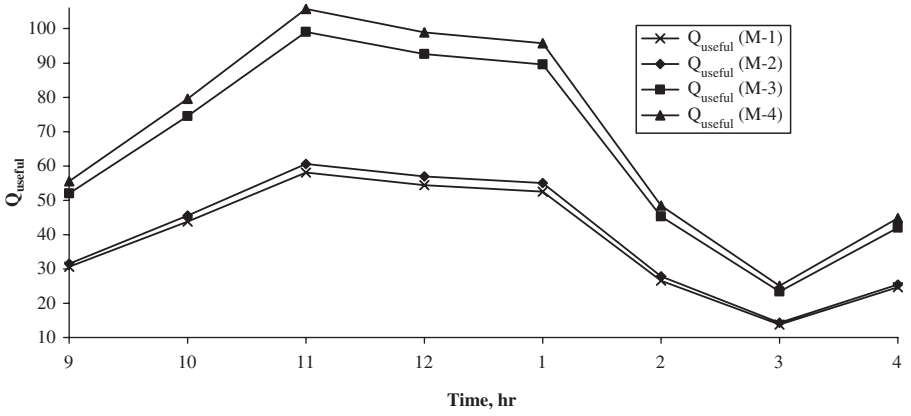

Fig. 7. Hourly variation of useful thermal energy with time.

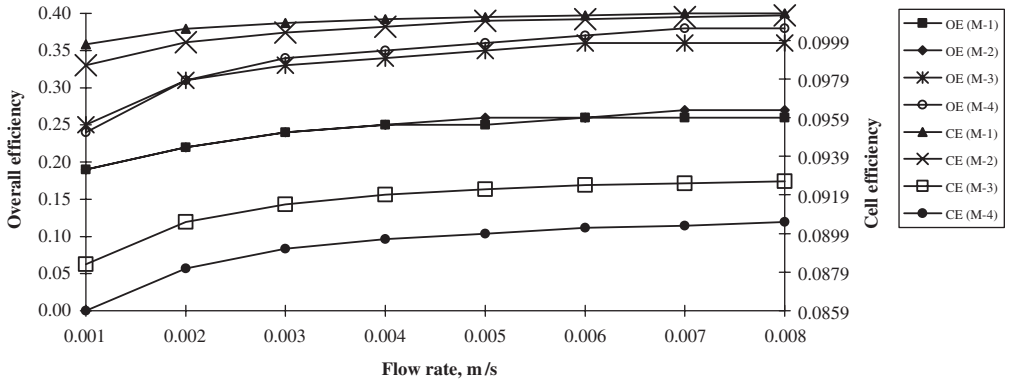

Fig. 8. Variation of an overall and cell efficiencies with flow rate for 1.2 m length hybrid PV/thermal system.

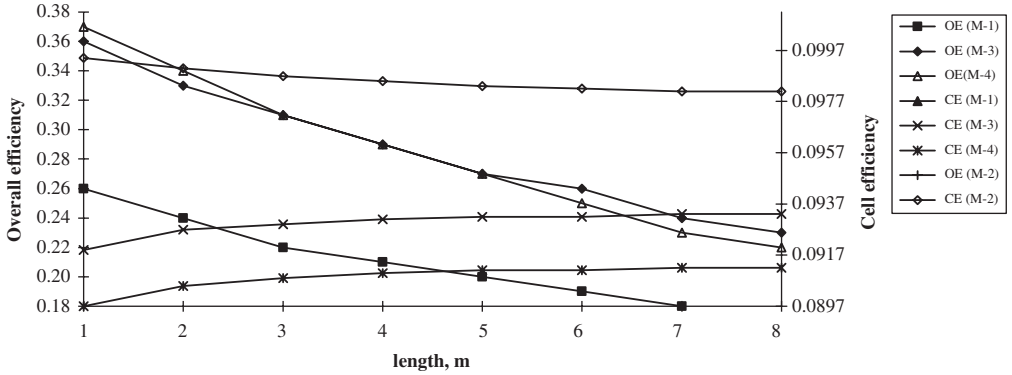

Fig. 9. Variation of an overall and cell efficiency with length for 0.005 m/s flow rate of hybrid PV/thermal system.

reduction in top loss coefficient, U_t for both cases as given by Eqs. (5a) and (5b). Further, the outlet air temperature (T_{airout}), back surface of module (T_{bs}) and solar cell (T_c) temperatures for module IV without tedlar is slightly higher than the values for module III with tedlar as expected. It is to be noted that there will not be back surface temperature in Fig. 6b due to absence of tedlar for modules II and IV, respectively.

The rate of useful thermal energy obtained from PV/T system has been computed from Eq. (8) for all four cases and its variation with time has been shown in Fig. 7. In this case too, the rate of useful thermal energy obtained from PV/T system for glazed hybrid PV/T, modules III and IV is higher than other two cases namely unglazed hybrid PV/T system as expected. The other conclusion for with and without tedlar remains the same.

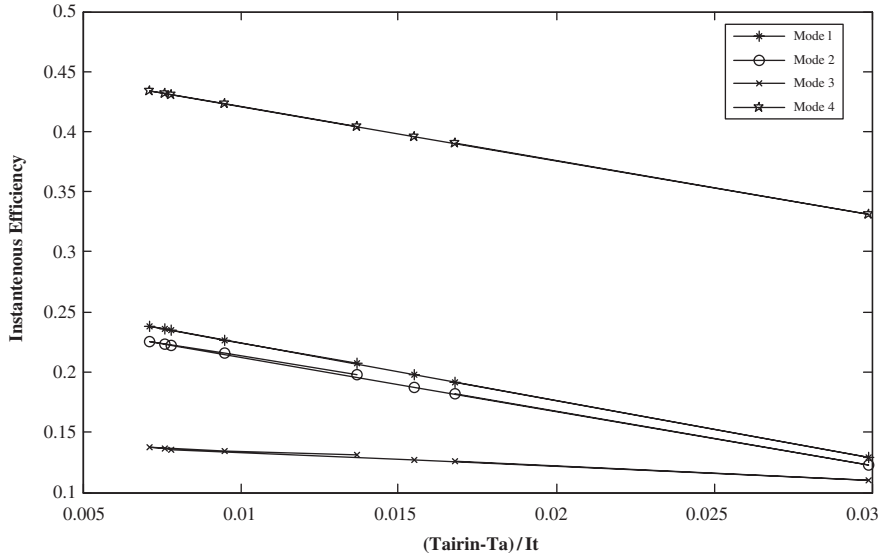

Fig. 10. Variation of instantaneous efficiency.

Effect of mass flow rate for a given length of PV module on an overall efficiency of hybrid PV/T system (Eq. (9)) and electrical efficiency (Eq. (7b)) have been shown in Fig. 8. It can be observed that an overall efficiency and electrical efficiency of hybrid PV/T system increases with an increase of mass flow rate. It is due to the fact that as mass flow rate increases; the withdrawal of heat also increases along with reduction in temperature of the system, which causes the increase in electrical efficiency.

Fig. 9 shows the effect of length of the PV module on an overall efficiency and an electrical efficiency of hybrid PV/T system for all configurations. It may be noted that an overall efficiency and an electrical efficiency of hybrid PV/T system decreases with an increase of length of the hybrid PV/T system due to an increase in the operating temperature range of the hybrid PV/T system as expected.

4.3. Testing procedure

Eq. (10) has been computed for all configurations for $T_{\text{airin}} = T_{\text{a}} + 5$ and the variation between η_{i} and $(T_{\text{airin}} - T_{\text{a}})/I(t)$ has been shown in Fig. 10. It is very much clear that module IV, glazed without tedlar, Fig. 1d, gives the best performance among others.

4.4. Two hybrid PV/T module (L_1) connected in series for given length, $L = 2L_1$

In this case, numerical calculations for glazed PV/T without tedlar have been carried out and the results for hourly variation of the solar cell (T_{c}) the outlet air temperature (T_{airout}) and the rate of useful (Q_{u}) energy have been shown in Fig. 11. It is to be noted that the solar cell (T_{c}) for single module is significantly increased in the case of the two-module system due to an increase in the inlet temperature of the second module as expected (Fig. 11a). However, there is marginal increase in outlet air temperature as shown in Fig. 11b. There is an overall decrease in the rate of useful energy (sum of the rate of useful energy from modules I and II, Fig. 11c) because of an increase in the solar cell temperature, which is responsible for the decrease in an overall electrical ($\eta_{\text{E}} = 12\%$) and thermal efficiency ($\eta_{\text{TH}} = 25\%$) by 2% from 39% to 37%. If conversion factor from electrical to thermal is considered as in Eq. (9c), then

$$\eta_{\text{O}} = \left[\frac{0.12}{0.40} + 0.25\right]100 = 30 + 25 = 55\%.$$

This indicates an increase of about 22% in an overall thermal efficiency.

5. Conclusion

On the basis of the present study, one can infer that the glazed hybrid PV/T system without tedlar, model IV, is the best system among others with significant increase in an overall efficiency (Fig. 10) which can be used for various applications namely space heating, water heating, drying, greenhouse, illumination and lighting, etc. Other conclusions are as follows:

(i) There is no difference in the solar cell temperature of unglazed PV/T module with, Model I, and without tedlar, Model II (Fig. 6a). However, there is marginal increase in outlet air temperature in model IV due to absence of tedlar.
(ii) An overall efficiency of hybrid system and solar cell efficiency increases with increase of mass flow rate of air through the duct due to reduction in losses from the system (Fig. 8).

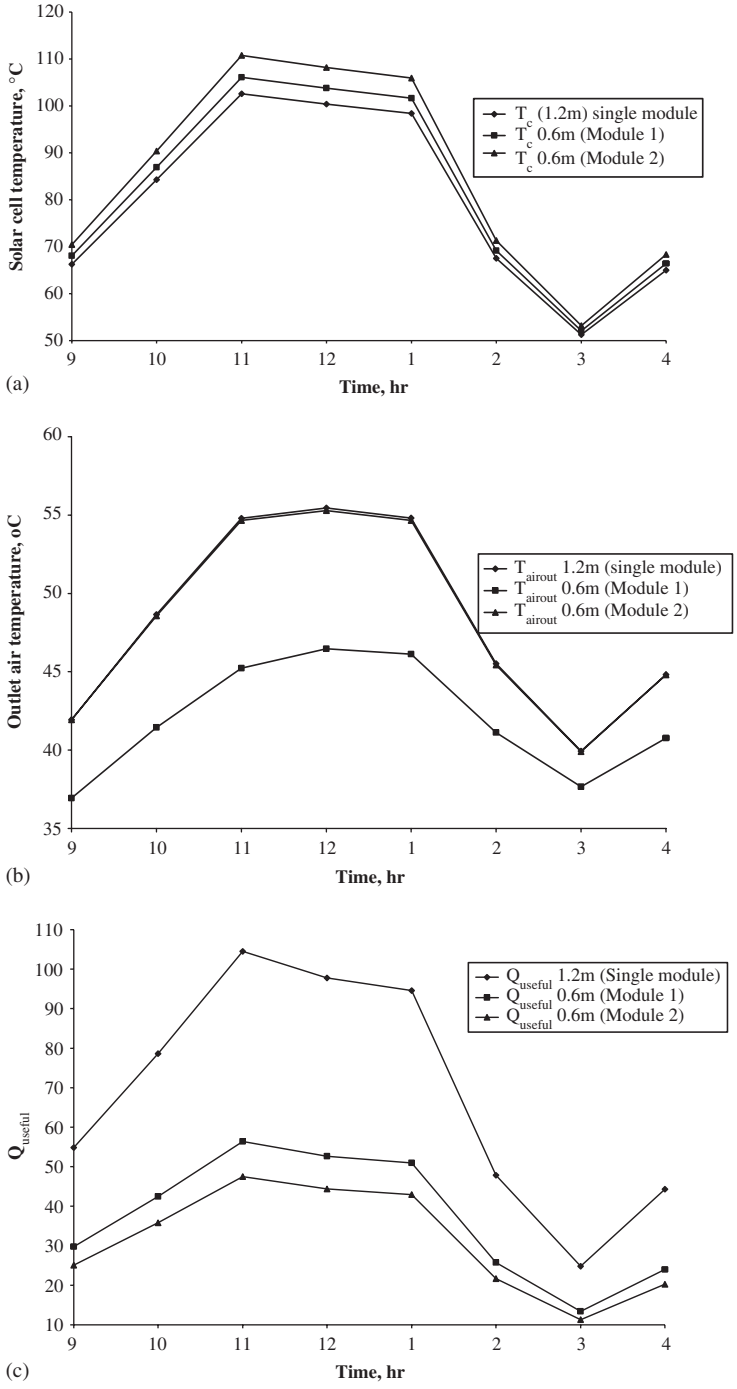

Fig. 11. (a) Variations of solar cell temperature with time. (b) Variations of outlet air temperatures with time. (c) Variations of rate of useful thermal energy with time.

(iii) An overall efficiency of the hybrid system decreases with an increase of the length of the module due to more losses from the system (Fig. 9). However, solar cell efficiency increases due to decrease in temperature as expected.

(iv) There is significant increase in an overall efficiency of the hybrid PV/T system if more small modules are connected in series for a given length of the system.

References

[1] A.D. Jones, C.P. Underwood, Sol. Energy 70 (4) (2001) 349.
[2] H.A. Zondag, D.W. de Vries, W.G.J. van Helden, R.J.C. van Zolengen, A.A. van steenhoven, Sol. Energy 72 (2) (2002) 113.
[3] S.A. Kalogirou, Renew. Energy 23 (2001) 247.
[4] H.P. Garg, R.K. Agarwall, J.C. Joshi, Energy Convers. Manage. 35 (1994) 621.
[5] T.T. Chow, Sol. Energy 75 (2003) 143.

[6] Y. Tripanagnostopulos, T.H. Nousia, M. Souliotis, P. Yianoulis, Sol. Energy 72 (3) (2002) 217.
[7] R. Zakharchenko, L. Licea-Jime'nez, S.A. Pe'rez-Garci'a, P. Vorobiev, U. Dehesa-Carrasco, J.F. Pe'rez-Robels, J. Gonza'lez-Herna'ndez, Y. Vorobiev, Sol. Energy Mater. Sol. Cell 82 (1–2) (2004) 253.
[8] B. Sandnes, J. Rekstad, Sol. Energy 72 (1) (2002) 63.
[9] A.A. Hegazy, Energy Convers. Manage. 41 (8) (2000) 861.
[10] D. Infield, L. Mei, U. Eicker, Sol. Energy 76 (1–3) (2004) 93.
[11] J. Prakash, Energy Convers. Manage. 35 (1994) 967.
[12] B.P. Cartmell, N.J. Shankland, D. Fiala, V. Hanby, Sol. Energy 76 (2004) 45.
[13] E. Radziemska, Progr. Energy Combust. Sci. 29 (2003) 407.
[14] M. Bosonac, B. Sorensen, I. Katic, H. Sorensen, B. Nielsen, J. Badran, Photovoltaic/thermal solar collector and their potential in Denmark, Final Report EEP Project 1713/00-0014, 2003, p. 28. 〈www.solenergi.dk/rapporter/pvtpotentialindenmark.pdf〉.
[15] M.J. Moran, Engineering Thermodynamics. LCC, CRC Press, Boca Raton, FL, 1999 (Chapter II).
[16] A. Tiwari, M.S. Sodha, A. Chandra, J.C. Joshi, Sol. Energy Mater. Sol. Cells 90 (2) (2006) 175.
[17] T. Schott, Sol. Energy 5 (1987).
[18] D.L. Evans, Sol. Energy 33 (6) (1984).